Mechanisms of Climate Warming at the End of the Paleocene

Santo Bains,[1]* Richard M. Corfield,[1] Richard D. Norris[2]

An abrupt episode of global warming marked the end of the Paleocene epoch. Oxygen and carbon isotope records from two widely separated sites support the notion that degassing of biogenic methane hydrate may have been an important factor in altering Earth's climate. The data show evidence for multiple injections of methane, separated by intervals in which the carbon cycle was in stasis. Correlations between the two sites suggest that even these small-scale events were global in nature.

Earth's climate warmed dramatically 55.5 million years ago during an event known as the Late Paleocene thermal maximum (LPTM) (*1*). Taxonomic turnover increased (*2*, *3*) during this, the warmest interval of the Cenozoic, with many modern mammal groups appearing and archaic lineages dying out (*4*).

Ocean carbon isotope ($\delta^{13}C$) (*5*) values dropped by 2.5 per mil (‰) at the onset of the LPTM (*2*, *6*–*9*), implying that there was a large input of isotopically negative carbon to the ocean and atmosphere. Although volcanic degassing could contribute CO_2 (*1*, *6*, *10*, *11*), current knowledge suggests that the rapidity and amplitude of the carbon isotope event (CIE) and the LPTM can only be explained by the dissociation of a large volume of methane from hydrates buried on continental shelves (*12*, *13*). Methane from this source has an average $\delta^{13}C$ of −60‰ because of its biogenic origin (*14*) and is also an efficient greenhouse gas (as is its oxidation product, CO_2) (*15*). The magnitude and duration of carbon flux and climatic change across the LPTM are the only known examples in the Cenozoic record that may approximate the pace of industrial anthropogenic emissions.

It has been suggested that global warming could induce positive feedback, whereby accumulations of methane hydrate degas into the ocean and atmosphere as thermal stability regimes are altered (*8*, *13*), driving further global warmth. Here we present detailed stable isotope data that document the mechanisms of such an event. Globally correlative features within the CIE show that minimum $\delta^{13}C$ values were reached in a stepped manner, which suggests a pulsed liberation of methane from the sea floor.

We measured the $\delta^{13}C$ and $\delta^{18}O$ composition of bulk carbonates from Ocean Drilling Program (ODP) sites 690B (Maud Rise, Weddell Sea, Antarctica, 65°09′S, 01°12′E) and 1051B (Blake Nose, western North Atlantic Ocean, 30°03′N, 76°21′W) (Fig. 1) at a sample resolution of 1 to 2 cm across the LPTM using standard techniques (*16*). Bulk carbonate measurements are sensitive to variations in nanofossil taxonomic composition and size fractions as well as diagenesis. However, we are confident that these considerations do not affect the fidelity of our (particularly $\delta^{13}C$) data, because (i) the records correlate well between sites 690B and 1051B, and both maintain a high $CaCO_3$ content throughout the excursion interval (>55%) (*17*, *18*); (ii) bulk isotope stratigraphy has been used to accurately reconstruct sea surface conditions of the Pleistocene (*19*); (iii) our site 690B bulk data correlate well with foraminifera data from the same site (Fig. 2); and (iv) scanning electron microscope observations (*17*) show approximately equal proportions of placolith and discoaster platelets across the LPTM interval in both sites. Nanofossils from these samples do not show evidence of significant infilling and recrystallization.

The LPTM and CIE are located in the long reversed-polarity zone termed magnetochron 24R (duration, ~2.557 million years) (*20*), which makes intersite correlation around the LPTM interval difficult (*21*). Age models based on nanofossil and planktonic foraminifera datums are inadequate to define these events, because they span a fraction of the duration of the biostratigraphic zones in which they take place (*18*). Estimates for CIE duration vary greatly; however, its onset is commonly believed to have occurred over only ~10,000 years (*6*, *8*). A decline in $CaCO_3$ across the CIE in many deep sea and shelf sites has given rise to the suggestion that dissolution leads to substantial underestimation of the event's duration (*22*). However, $CaCO_3$ data from sites 690B and 1051B (*17*, *18*) do not show significant dissolution coincident with the CIE, and lithologic observations do not indicate a hiatus over this interval. To better constrain LPTM duration, we used a time scale based on the residence time of carbon in the ocean and atmosphere (*23*). Additionally, we plotted our isotope data in meters below the sea floor (mbsf).

Our bulk isotopic data are presented in Fig. 2 together with published foraminiferal records (*6*). The amplitude of the CIE in bulk sediment is identical to the magnitude of the excursion in deep-dwelling planktonic and benthic foraminifera, which suggests that our bulk isotope record accurately reflects changes in the whole-ocean reservoir of dissolved carbon. The higher amplitude of the surface-dwelling *Acarinina* record, and its faster recovery to near pre-excursion values, may be related to this taxon's possession of photosymbionts (*24*).

Starting ~300,000 years before the CIE, $\delta^{13}C$ and $\delta^{18}O$ records trend gradually toward negative values (a, Fig. 2). However, between 171.36 and 170.64 mbsf, at site 690B there is a reversal in both $\delta^{18}O$ and $\delta^{13}C$ (b, Fig. 2). The $\delta^{18}O$ values increase by ~1‰, which suggests a drop in high-latitude sea surface temperature (SST) of ~4°C, whereas $\delta^{13}C$ values increase by ~0.8‰. The onset of the CIE in site 690B is a very rapid negative shift of greater than 1‰ (c, Fig. 2) and is coincident with a $\delta^{18}O$ excursion of similar magnitude. After the initial negative shift, both $\delta^{13}C$ and $\delta^{18}O$ records in site 690B level out (d, Fig. 2). A second negative $\delta^{13}C$ and $\delta^{18}O$ excursion (e, Fig. 2) follows this transient plateau. Although not as abrupt as the primary carbon isotope excursion (c, Fig. 2), its magnitude is almost as great (~1‰ for $\delta^{13}C$ and $\delta^{18}O$). After this second excursion (e, Fig. 2), records level out and inflect slightly toward more positive values (f, Fig. 2).

A third and final negative shift in $\delta^{13}C$ and $\delta^{18}O$ occurs at both sites (g, Fig. 2). This

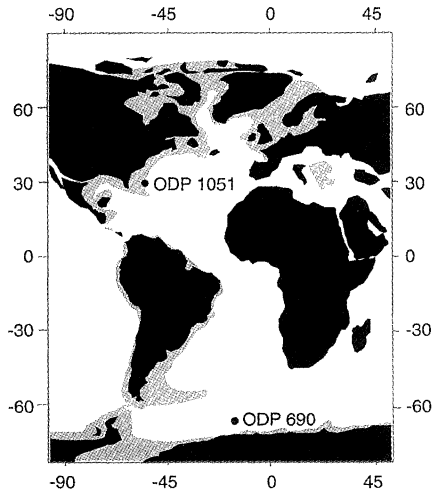

Fig. 1. World map showing the Paleocene location of the ODP sites discussed in this study.

[1]Department of Earth Sciences, Oxford University, Parks Road, Oxford, OX1 3PR, UK. [2]Department of Geology and Geophysics, Woods Hole Oceanographic Institution, Woods Hole, MA 02543, USA.

*To whom correspondence should be addressed. E-mail: Santo.Bains@earth.ox.ac.uk

shift in isotope values is smaller in magnitude than the two previous excursions and apparently spans a longer time interval. After this, $\delta^{13}C$ and $\delta^{18}O$ increase exponentially toward pre-excursion levels (h, Fig. 2). A final inflection in the records (i, Fig. 2) occurs at about 169.15 and 512.24 mbsf in sites 690B and 1051B, respectively, when values abruptly stabilize.

Dickens *et al.* (*12*) suggest that as latitudinal geothermal gradients reached a minimum at the end of a steady Late Paleocene warming trend (*6*, *9*, *10*, *25*), sinking warm waters pushed submarine methane hydrates beyond their dissociation threshold. A reversal in the predominant mode of ocean deep water circulation may have been triggered by CO_2 outgassing from circum-Caribbean volcanism that began before the LPTM (*8*). Coincident with the onset of the $\delta^{13}C$ excursion, benthic foraminifera suffered a major extinction, in which up to 50% of species perished [the benthic foraminifera extinction event (BEE)]. These organisms were probably poisoned by the introduction of unusually saline deep water (*9*) or by oxygen depletion due to a combination of increased warmth of the oceans (*25*) and the oxidation of liberated methane (*13*), or both. Degassing of methane into the ocean and atmosphere then induced global warming via greenhouse mechanisms.

Multiple $\delta^{18}O$ analyses of site 1051B ($n = 4$) confirm that there is virtually no change in the temperature of surface waters for ~150,000 years before the CIE (a, Fig. 2). The lack of evidence for surface water temperature change in site 1051B, coupled with evidence for surface and deep water cooling in site 690B (b, Fig. 2), seem inconsistent with suggestions that the crossing of a thermal threshold was the triggering mechanism

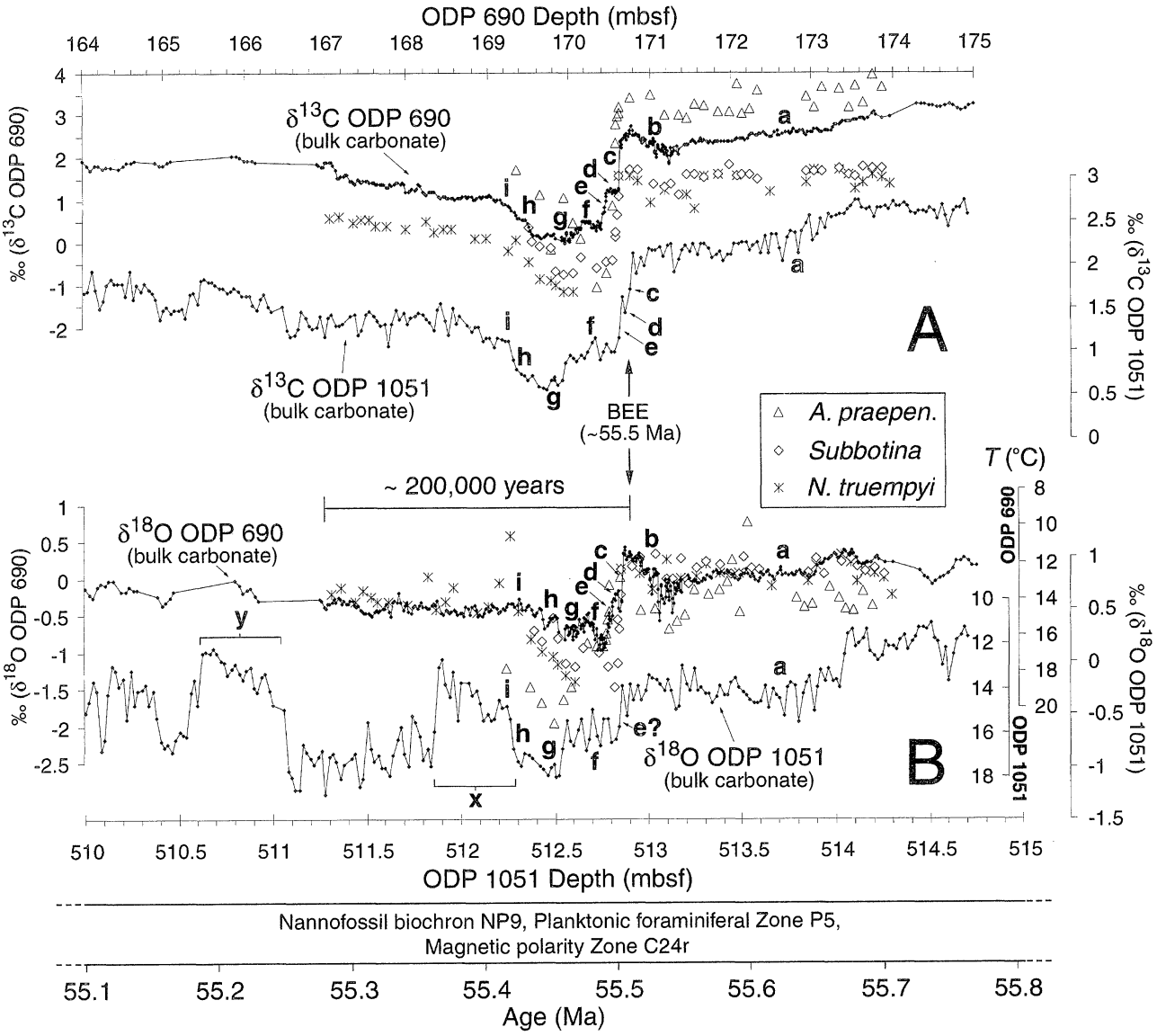

Fig. 2. The $\delta^{13}C$ and $\delta^{18}O$ records of marine bulk carbonate, planktonic foraminifera *Acarinina praepentacamerata* and *Subbotina*, and the benthic foraminifer *Nuttallides truempyi* across the LPTM interval in ODP sites 690B and 1051B (*6*). Labels a through i are used to denote events across the LPTM and are referred to in the text. Ma, million years ago. (**A**) Changes in $\delta^{13}C$ across this interval record a number of small-scale global carbon isotope fluctuations. The stepped fall in values suggests multiple injections of light carbon from dissociated methane or some other source. (**B**) The $\delta^{18}O$ records from these two sites are very similar across the LPTM; however, the oxygen isotope values may have been more strongly affected than the carbon isotope records by latitudinally dependant temperature-forcing mechanisms (for example, cyclic variation of Earth's orbit) and are thus less correlative than the $\delta^{13}C$ records. Features x and y probably represent enhanced episodes of low-latitude cooling associated with precessional periods. Temperatures were calculated with the method of Shackleton (*31*).

for methane hydrate dissociation. One possible explanation is that poleward heat transport may have changed from surface to deeper waters during the pre-excursion interval and thus caused high-latitude surface waters to cool, as they no longer received heat from the low latitudes (*26*). However, this would require ocean circulation reorganization ~30,000 years earlier than previous studies suggest (*6*, *9*, *10*). We propose that crossing a thermal threshold may not have been the initial cause of LPTM methane dissociation. Other possibilities could include submarine seismicity, volcanism, or simple gravitational slumping that induced catastrophic slope failure on continental margins rich in hydrate deposits. A drop in pressure can cause destabilization of methane hydrate accumulations (*12*). The Late Paleocene is believed to have been ice cap–free, and so a drop in pressure (global sea level) due to glaciation would be in contradiction to previous studies (*1*). However, our data do suggest a decrease in high-latitude surface water temperatures just before the CIE and could reflect a significant cooling of Antarctica.

The initial isotope excursion (c, Fig. 2) in site 1051B coincides precisely with the BEE. The $\delta^{13}C$ values decrease by ~1‰ within a 4-cm interval (somewhat less rapidly than the excursion observed in site 690B). Laminae are seen in the sediments from this part of the LPTM at both sites, which suggests that bioturbation is not a factor affecting the interpretation of the isotope records. However, it is possible that stable isotope records from site 1051B may have been affected by the presence of a clast layer that occurs immediately below the BEE. Although the initial $\delta^{18}O$ decline (inferred warming) in site 690B is synchronous with the first $\delta^{13}C$ decline (c, Fig. 2), in site 1051B it occurs later than the initial $\delta^{13}C$ excursion, even though the $\delta^{13}C$ excursion in both sites is synchronous. This offset is therefore probably real and represents a difference in the timing of surface water warming between the high and the low latitudes.

The plateau (d, Fig. 2) may represent a temporary period when addition of isotopically negative carbon to the ocean-atmosphere system halted. The equivalent feature in the site 1051B record is not as clearly defined, possibly because of the presence of the above-mentioned clast interval. The $\delta^{18}O$ data from site 690B show evidence of a temporary return to cooler values at the same time as methane degassing slowed.

The secondary stage of the $\delta^{13}C$ excursion (e, Fig. 2) probably represents another injection of isotopically negative carbon from dissociating methane hydrate. One possibility is that the transient plateau represents the time required for warm, saline, low-latitude water to mix into the deep sea and to heat sediment pore water (by conduction and advection) down to the methane hydrate stability zone, thus destabilizing a large accumulation of gas. However, we cannot discount the possibility that the second episode of methane outgassing may also have been induced by some other mechanism.

Feature f in Fig. 2 represents another possible temporary cessation of methane release. This is again accompanied by a cooling of high-latitude surface waters, a feature that is reflected in the lower latitude $\delta^{18}O$ record from site 1051B. We suggest that the plateaus between injection events could represent periods in which the system is returning to equilibrium, but because the residence time of carbon in the oceans is greater than the time between ventings (~8000 and ~12,000 years for features d and f respectively; Fig. 2), this period is a time of stasis in the carbon system.

Feature g in Fig. 2 is the final negative excursion associated with the CIE, when $\delta^{13}C$ declines more slowly than during the previous two excursions. After this, $\delta^{13}C$ and $\delta^{18}O$ records in both sites increased as isotopically light carbon was removed from the ocean-atmosphere system, probably by burial in the deep ocean. An inflection in our records (i, Fig. 2) may represent the return of the system to equilibrium at slightly lower values than those before the initial excursion, because the Late Paleocene–Early Eocene interval is characterized by an overall decline in $\delta^{13}C$ globally for reasons that remain enigmatic (*27*).

Given that methane hydrate accumulations are geographically diverse (*28*) and that they can occur across a broad range of depths (between ~920 to ~4000 m for the Late Paleocene) (*12*), it seems unlikely that their dissociation would take place simultaneously. Consequently, it is not surprising that detailed analysis of the structure of the LPTM reveals several episodes of isotopically negative carbon injection and related climatic change.

Using mass balance equations developed by Dickens *et al.* (*12*), we estimate that to cause the initial isotope excursion in our bulk carbonate records (c, Fig. 2) would have required an injection of ~600 gigatons (Gt) (*29*) of carbon from methane hydrates (over an interval of less than 1000 years). The second and third forcing episodes could be explained by subsequent input of ~500 Gt and ~300 Gt, respectively. This would suggest a total methane input over the LPTM interval of ~1500 Gt, which falls within the range suggested by Dickens *et al.* (*12*, *13*).

The coherence of the data sets from the two sites suggests that even the small-scale carbon and oxygen isotope fluctuations we have identified are of global significance. A consequence of this is that it is possible to accurately correlate geographically diverse sections to a resolution of a few thousand years in lower Cenozoic sediments.

References and Notes

1. J. C. Zachos, K. C. Lohmann, J. C. G. Walker, S. W. Wise, *J. Geol.* **101**, 191 (1993).
2. P. L. Koch, J. C. Zachos, P. D. Gingerich, *Nature* **358**, 319 (1992).
3. P. L. Koch, J. C. Zachos, D. L. Dettman, *Palaeogeogr. Palaeoclimatol. Palaeoecol.* **115**, 61 (1995); S. L. Wing, J. Alroy, L. J. Hickey, *ibid.*, p. 117; J. J. Hooker, in *Correlation of the Early Paleogene in Northwest Europe*, R. W. Knox, R. M. Corfield, R. E. Dunay, Eds. (Geological Society, London, 1996), pp. 205–218; W. C. Clyde and P. D. Gingerich, *Geology* **26**, 1011 (1998); G. Lu and G. Keller, *Palaeogeogr. Palaeoclimatol. Palaeoecol.* **117**, 211 (1995); D. C. Kelly, T. J. Bralower, J. C. Zachos, I. P. Silva, E. Thomas, *Geology* **24**, 423 (1996); D. C. Kelly, T. J. Bralower, J. C. Zachos, *Palaeogeogr. Palaeoclimatol. Palaeoecol.* **141**, 139 (1998).
4. M. C. Mass, M. R. L. Anthony, P. D. Gingerich, G. F. Gunnell, D. W. Krause, *Palaeogeogr. Palaeoclimatol. Palaeoecol.* **115**, 181 (1995).
5. Carbon and oxygen data are reported in δ values, where $\delta^{13}C$ (in per mil) = $[(^{13}C/^{12}C)_{sample}/(^{13}C/^{12}C)_{standard} - 1] \times 1000$, and $\delta^{18}O$ (in per mil) = $[(^{18}O/^{16}O)_{sample}/(^{18}O/^{16}O)_{standard} - 1] \times 1000$. Results were calibrated to PeeDee belemnite by reference to an in-house Carrara Marble standard.
6. J. P. Kennett and L. D. Stott, *Nature* **353**, 225 (1991).
7. T. J. Bralower *et al.*, *Paleoceanography* **10**, 841 (1995); R. M. Corfield and J. E. Cartlidge, *Terra Nova* **4**, 443 (1992); L. D. Stott, A. Sinha, M. Thiry, M.-P. Aubry, W. A. Berggren, in *Correlation of the Early Paleogene in Northwest Europe*, R. W. Knox, R. M. Corfield, R. E. Dunay, Eds. (Geological Society, London, 1996), pp. 381–399.
8. T. J. Bralower *et al.*, *Geology* **25**, 963 (1997).
9. D. K. Pak and K. G. Miller, *Paleoceanography* **7**, 405 (1992).
10. E. Thomas and N. J. Shackleton, in *Correlation of the Early Paleogene in Northwest Europe*, R. W. Knox, R. M. Corfield, R. E. Dunay, Eds. (Geological Society, London, 1996), pp. 401–441.
11. O. Eldholm and E. Thomas, *Earth Planet. Sci. Lett.* **117**, 319 (1993); G. Lu and G. Keller, *Mar. Micropaleontol.* **21**, 101 (1993); J. C. Zachos, L. D. Stott, K. C. Lohmann, *Paleoceanography* **9**, 353 (1994).
12. G. R. Dickens, J. R. O'Neil, D. K. Rea, R. M. Owen, *Paleoceanography* **10**, 965 (1995).
13. G. R. Dickens, M. M. Castillo, J. C. G. Walker, *Geology* **25**, 259 (1997).
14. K. A. Kvenvolden, *Chem. Geol.* **71**, 41 (1988).
15. ———, in *Gas Hydrates*, J.-P. Henriet and J. Mienert, Eds. (Geological Society, London, 1998), pp. 9–30.
16. Several hundred micrograms of sample were powdered and cleaned of organic contaminants with 10% H_2O_2 and acetone. Samples were then reacted at 90°C in a common phosphoric acid bath carbonate preparation system coupled to a PRISM mass spectrometer in the Department of Earth Sciences, University of Oxford. The average time between the reaction of samples was about 30 min, which is sufficient to completely react all carbonate phases. Analytical precision better than 0.1‰ for both carbon and oxygen isotopes was maintained throughout all analyses.
17. S. Bains, R. M. Corfield, R. D. Norris, unpublished data.
18. T. J. Bralower, E. Thomas, J. C. Zachos, *Geology* **26**, 671 (1998).
19. N. J. Shackleton, M. A. Hall, D. Pate, L. Meynadier, P. Valet, *Paleoceanography* **8**, 141 (1993).
20. W. A. Berggren, D. V. Kent, C. C. Swisher III, M.-P. Aubry, in *Geochronology, Time Scales and Stratigraphic Correlations: A Unified Temporal Framework for an Historical Geology*, W. A. Berggren, D. V. Kent, M.-P. Aubry, J. Hardenbol, Eds. (Society for Economic Paleontologists and Mineralogists, Tulsa, OK, 1995), pp. 129–212.
21. W. A. Berggren and M.-P. Aubry, in *Correlation of the Early Paleogene in Northwest Europe*, R. W. Knox, R. M. Corfield, R. E. Dunay, Eds. (Geological Society, London, 1996), pp. 309–352.
22. G. R. Dickens, *Geology* **26**, 670 (1988).

23. Our time scale is based on a carbon cycling model that assumes that a steady removal of light carbon from the oceans and atmosphere will occur after an initial input of isotopically negative $\delta^{13}C$. Reequilibration of the ocean $\delta^{13}C$ signature will occur in an exponential fashion, according to published equations (*30*). The general shape of our $\delta^{13}C$ records suggests that this mechanism is at work during the LPTM and hence provides us with an independent first-order estimate of time. Because the residence time of carbon is ~100,000 years (also referred to as the e-folding time), it is possible to deduce the duration of small-scale events within the CIE by close examination of our records. After two e-folding times, the CIE signal should be reduced to within ~14% of its pre-excursion levels. We have estimated this ~200,000-year interval in Fig. 2 while taking into account the extended duration of methane injection and the negative $\delta^{13}C$ trend that persists well into the Early Eocene. The onset of the CIE is assigned an age of 55.5 million years ago (*20*), which coincides precisely with the BEE in both sites. We assumed constant sedimentation rates before, during, and after the CIE.
24. R. M. Corfield and R. D. Norris, in *Late Paleocene–Early Eocene Climatic and Biotic Events in the Marine and Terrestrial Records*, M.-P. Aubry, S. G. Lucas, W. A. Berggren, Eds. (Columbia Univ. Press, New York, 1998), pp. 124–137.
25. E. Thomas, *Proc. Ocean Drilling Prog. Sci. Results* **113**, 571 (1990).
26. T. F. Stocker and A. Schmittner, *Nature* **388**, 862 (1997)
27. R. M. Corfield, *Earth Sci. Rev.* **37**, 225 (1994).
28. J. S. Booth, W. J. Winters, W. P. Dillon, M. B. Clennell, M. M. Rowe, in (*15*), pp. 113–128.; G. D. Ginsburg, in (*15*), pp. 61–62.; B. U. Haq, in *Gas Hydrates*, J.-P. Henriet and J. Mienert, Eds. (Geological Society, London, 1998), pp. 303–318.
29. One gigaton = 1×10^{15} g.
30. W. H. Berger and E. Vincent, *Geol. Rundsch.* **75**, 249 (1986).
31. N. J. Shackleton, in *Fossils and Climate*, P. J. Brenchley, Ed. (Wiley, New York, 1984), pp. 27–34.
32. We thank J. Cartlidge and S. Wyatt for their expert help in the operation of the mass spectrometers in the Stable Isotope Laboratory at Oxford and O. Green, D. Patrick, W. Hale, M. Bowman, P. Weiss, and J. Firth for assistance. This work was supported by the Natural Environment Research Council (U.K.), scholarship number GT4/97/214/ES.

29 March 1999; accepted 28 May 1999

Activation of NK Cells and T Cells by NKG2D, a Receptor for Stress-Inducible MICA

Stefan Bauer,[1]*† Veronika Groh,[1]* Jun Wu,[2] Alexander Steinle,[1] Joseph H. Phillips,[2] Lewis L. Lanier,[2] Thomas Spies[1]‡

Stress-inducible MICA, a distant homolog of major histocompatibility complex (MHC) class I, functions as an antigen for γδ T cells and is frequently expressed in epithelial tumors. A receptor for MICA was detected on most γδ T cells, $CD8^+$ αβ T cells, and natural killer (NK) cells and was identified as NKG2D. Effector cells from all these subsets could be stimulated by ligation of NKG2D. Engagement of NKG2D activated cytolytic responses of γδ T cells and NK cells against transfectants and epithelial tumor cells expressing MICA. These results define an activating immunoreceptor-MHC ligand interaction that may promote antitumor NK and T cell responses.

Major histocompatibility complex class I molecules are ligands for inhibitory or activating natural killer (NK) cell receptors that are expressed on NK cells and T cells. These include isoforms of the immunoglobulin (Ig)-like killer cell receptors that interact with HLA-A, -B, or -C, and CD94 paired with NKG2A or NKG2C, which bind HLA-E (*1–4*). Engagement of these receptors modulates NK cell responses and T-cell antigen receptor (TCR)-dependent T-cell activation (*1, 5*).

Expression of MHC class I is frequently impaired in virus-infected or tumor cells, which results in lack of engagement of inhibitory receptors and thus activation of NK cells (*1, 6*). Hence, class I serves as a positive indicator for the integrity of cells, protecting against NK cell attack. In contrast, MICA and its close relative MICB may signal cellular distress and evoke immune responses. These molecules function as stress-inducible antigens in intestinal epithelium and are recognized alike by γδ T cells with the TCR variable region $V_\delta1$ (*7, 8*). In addition, they are frequently expressed in epithelial tumors including lung, breast, kidney, ovary, prostate, and colon carcinomas (*9*). We investigated receptor interactions of MICA.

A soluble form of MICA (sMICA) including the α1α2α3 extracellular domains was expressed and purified (*10*). Addition of sMICA to cytotoxicity assays inhibited the responses of several $V_\delta1$ γδ T-cell clones to C1R cell transfectants expressing MICA (Fig. 1A) (*8, 11*). We investigated whether this effect was associated with expression of the γδ TCRs alone or involved surface molecules that occurred separately. Flow cytometry showed binding of biotinylated sMICA (bio-sMICA) to several $V_\delta1$ γδ T-cell clones (*10*). However, stainings of peripheral blood lymphocytes (PBLs) revealed binding of bio-sMICA to most γδ T cells (of the $V_\delta1$ and $V_\delta2$ subsets), $CD8^+$ T cells, and $CD56^+$ NK cells, but only to a few $CD4^+$ T cells. The cell lines NKL (NK cell) and Hut 78 (T cell) were positive, whereas CEM, Jurkat, HPB-ALL, MOLT4, and PEER (T cells), and Daudi and Raji (B cells) were negative (*10, 12*). These interactions were analyzed with monoclonal antibodies (mAbs) that were screened for binding specificities matching those of bio-sMICA (*10*). Two selected mAbs, 5C6 and 1D11, stained NKL and the $V_\delta1$ γδ T-cell clones and blocked binding of bio-sMICA (Fig. 1, C and D). As with sMICA, both mAbs inhibited T-cell recognition of MICA (Fig. 1B). With PBLs from several individuals, the distribution of epitopes recognized by these mAbs replicated the staining pattern of bio-sMICA (Fig. 2) (*10*). The mAbs 5C6 and 1D11 cross-blocked surface binding (*13*). Thus, MICA interacted with a surface receptor (MICR) that was widely distributed on lymphocyte subsets.

To identify MICR, we used representational difference analysis (RDA) (*14*). Representations of cDNAs were prepared from pools of $CD4^+$ T-cell clones that were positive or negative for MICR expression. Three rounds of hybridization-subtraction and amplification yielded a representational difference product (RDP) of five DNA fragments. Four of these probably were not relevant. The most prominent fragment matched the sequence of NKG2D, which is an orphan C-type lectin-like NK cell receptor of unknown expression and function (Fig. 3A) (*15*).

NKG2D was scrutinized as a candidate for MICR. Blot hybridization confirmed the presence of NKG2D mRNA in NKL and Hut 78 cells, as well as in a $V_\delta1$ γδ T cell line and in $CD8^+$ T cells isolated from PBLs (Fig. 3B) (*16*). A second transcript of higher molecular weight presumably corresponded to a transcriptional variant of NKG2D. In contrast, little or no mRNA was detected in Jurkat, HPB-ALL, and peripheral blood $CD4^+$ T cells. Thus, the distribution of NKG2D mRNA, which was in accord with previous limited data (*15*), matched the expression of MICR. Immunoprecipitations with mAbs 5C6 and 1D11 identified a single surface protein that was expressed on NKL and Hut 78 but not on Jurkat cells (Fig. 3C). Its apparent molecular mass of 42 kD matched

[1]Fred Hutchinson Cancer Research Center, Clinical Research Division, 1100 Fairview Avenue North, Seattle, WA 98109, USA. [2]DNAX Research Institute of Molecular and Cellular Biology, Palo Alto, CA 94304, USA.

*These authors contributed equally to this work and are listed in alphabetical order.

†Present address: Technical University of Munich, Institute of Microbiology, Trogerstrasse 32, D-81675 Munich, Germany.

‡To whom correspondence should be addressed. E-mail: tspies@fred.fhcrc.org